ELSEVIER

Physica D 80 (1995) 256–276

PHYSICA D

Nonmonotonic twist maps ★

James E. Howard, Jeffrey Humpherys

Department of Mathematics and Statistics, Utah State University, Logan, UT 84322-3900, USA

Received 31 March 1994; revised 3 August 1994; accepted 3 August 1994
Communicated by J.D. Meiss

Abstract

We investigate a family of nonmonotonic radial twist maps constructed by unfolding the linear twist function. We find several new modes of reconnection and derive conditions for them to occur. Reconnection and bifurcation of higher order resonances are studied in detail, including vortex pairs and triplets. The structural instability of some of these exotic figures is mitigated by the presence of chaotic separatrix layers. Invariant curves of involution pairs are utilized to locate and chart their often very complex metamorphoses.

1. Introduction

Radial twist maps of the form

$$T: \begin{cases} x' = x - K\sin\theta, \\ \theta' = \theta + f(x'), \end{cases} \tag{1}$$

where the *twist function* $f(x)$ is smooth in some interval, are often encountered in physical problems. For example, the choice $f(x) = x$ gives the standard map [1], while $f(x) = 1/x$ yields the Fermi map [2]. Usually $f(x)$ is monotonic in the interval of interest, but occasionally one finds situations where $f(x)$ possesses an extremum, $f'(x) = 0$. Important instances include orbits in particle accelerators [3], plasma wave heating [4], and fluid dynamics [5]. Such mappings have many novel properties, as a consequence of the degeneracy of the unperturbed motion. Formally regarding K as a perturbation parameter, the mapping (1) may be derived from the generating function

$$\begin{aligned} S(x',\theta) &= S_0(x') + KS_1(x',\theta) \\ &= \int^{x'} f(\xi)\,d\xi + K\sin\theta \end{aligned} \tag{2}$$

so that $\partial\omega/\partial x = \partial^2 S_0/\partial x^2 = 0$ whenever $f'(x) = 0$. Violation of nondegeneracy means that most of the familiar lynchpins of Hamiltonian dynamics are inapplicable, including the Poincaré–Birkhoff theorem [6], the Moser twist theorem [7], and the KAM theorem [8,9]. Nevertheless, owing to the continuity of the mapping (1) the Poincaré index is conserved, limiting the types of bifurcations that can occur [1].

In a previous paper [10] we studied the properties of a one-parameter class of maps for which the twist function $f(x;\alpha)$ possesses a single local maximum. For this class of nonmonotonic twist maps [2] we

★ This paper is dedicated to the memory of Jeffrey Tennyson.

[1] A familiar example of a violation of the Poincaré index is the bifurcation of the central island in the standard map as K passes through zero to negative values. In the present case we avoid this possibility by restricting K to positive values.

[2] Some authors use the term "non-twist" to describe maps for which the twist condition is violated at isolated points.

0167-2789/95/$09.50 © 1995 Elsevier Science B.V. All rights reserved
SSDI 0167-2789(94)00180-4

showed that the period-one primary resonances occur in pairs, with island centers staggered 180^o in phase, i.e., each pair of resonances has opposite type and is situated at the same phase. We also found that as a control parameter was varied the intervening KAM curves could *reconnect* at a critical parameter value, as depicted in Fig. 1. Here we shall define reconnection of a flow or a discrete mapping as a topological rearrangement of integral curves in which the critical points do not change their Morse type. Note that this definition does not preclude the creation of additional critical points dictated by preservation of the Poincaré index. We shall refer to the sharing of separatrices seen in Fig. 1b as *braiding*. From the averaged Hamiltonian[3],

$$\bar{H} = \int_{x_n}^{x} [f(\xi;\alpha) - 2\pi n]\,d\xi - K\cos\theta, \tag{3}$$

valid in the neighborhood of a resonance, $f(x_n) = 2\pi n$, it follows that reconnection of two contiguous separatrices occurs when

$$K(\alpha) = \tfrac{1}{2}\int_{x_1}^{x_2} [f(\xi;\alpha) - 2\pi n]\,d\xi. \tag{4}$$

This gives an approximate condition for the reconnection of separatrix *layers* in the map (1). In applying this formula, account must be taken of bifurcations, which may be analyzed with the help of the tangent map

$$\mathcal{L} = DT = \begin{pmatrix} 1 & -K\cos\theta \\ f' & 1 - Kf'\cos\theta \end{pmatrix}. \tag{5}$$

Thus, when $\operatorname{Tr}\mathcal{L} = 2 - Kf'\cos\theta = +2 \Rightarrow f' = 0$, adjacent elliptic and hyperbolic fixed points annihilate in a tangent bifurcation, as depicted in Fig. 1d. When $\operatorname{Tr}\mathcal{L} = -2$, a period-doubling bifurcation occurs, in which case the notion of reconnection becomes meaningless. It is also worth noting that the map (1) may be written as a product of involutions, $T = I_2 I_1$, with $I_1^2 = I_2^2 = I$ as follows:

[3] Note that the Legendre condition, $\partial^2\bar{H}/\partial x^2 = 0$ is violated for this approximate Hamiltonian.

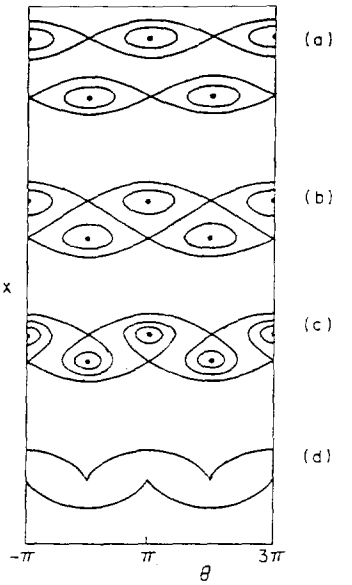

Fig. 1. Reconnection scenario for quadratic nonmonotonic twist map (two periods are shown for clarity).

$$I_1 : \begin{cases} x' = x - K\sin\theta, \\ \theta' = -\theta, \end{cases} \tag{6a}$$

$$I_2 : \begin{cases} x' = x, \\ \theta' = -\theta + f(x'). \end{cases} \tag{6b}$$

The decomposition (6) implies that the mapping T is *reversible* [11,17], i.e. there exists a symmetry S such that $T^{-1} = STS$. Explicitly, $S = I_2$, so that $T^{-1} = I_1 I_2$. This does not mean, however, that the Hamiltonian (3) is time-reversal invariant, although the converse implication holds. Indeed, we shall see that for the mappings considered in this paper H is not even in the momentum. In Section 5 we shall use the invariant curves of I_1 and I_2 for analyzing reconnections and bifurcations of higher order resonances.

Recently several authors have studied the reconnection process in some detail. In one paper, reconnection was found to occur near the 1:3 resonance in the Hénon map [12]. For a certain parameter range, the rotation number was found to have an extremum away from the central resonance, leading to the formation of twin Poincaré–Birkhoff chains. In a sequel [13], a rather complicated map was constructed, for which reconnection takes place in stages. The effects of a small amount of dissipation on the reconnection/bifurcation

scenario were also investigated, and in more detail in Ref. [14], which also considered flows as well as discrete maps. Reconnecting flows in two degrees of freedom were also studied for a cubic model Hamiltonian derived from a general Birkhoff normal form expansion [15]. Poincaré sections were calculated numerically for a 1:6 resonance including both integrable and nonintegrable perturbations.

In this paper we introduce a family of nonmonotonic twist maps constructed by adding lower order polynomials to the linear twist function in the standard map. Section 2 describes the general family of twist maps under consideration and reviews previous work on the quadratic case. Section 3 contains a detailed account of the interaction of the period-one islands in the cubic twist map. The possible reconnection scenarios are classified and described in quantitative detail. A set of reconnection thresholds analogous to (4) are derived and found to compare well with numerical maps. As in the mapping model of van der Weele and Valkering [12] and the model flow of de Carvalho and de Almeida [15], we find that reconnection takes place in stages as a control parameter is varied. However, the relative simplicity of our mappings allows us to describe new types of braiding and reconnection analytically. Moreover, the polynomial twist functions considered here are natural extensions of linear twist, which may well have physical manifestations. Section 4 contains a brief discussion of the quartic twist map, which has less symmetry than the quadratic or cubic maps.

Section 5 compares the behavior of the higher-order primary resonances in the quadratic and cubic twist maps. While many similar bifurcations and reconnections are observed, there are important differences. Thus, higher-order loops are observed to form and disappear, but now *even*-order loops, which bifurcate asymmetrically, are seen for cubic twist. In both cases the period-two islands form vortex pairs, similar to those observed in hydrodynamics. With the help of the invariant curves of T^2 we obtain explicit conditions for their formation and subsequent destruction in the case of quadratic twist and semi-analytically for cubic twist. An approximate period-two Hamiltonian, which correctly describes vortex pair formation for $\alpha K^2 \ll 1$ is obtained via secular perturbation theory. In addition to vortex pairs, we also predict and observe vortex *triplets* in the cubic map. Although triplets are structurally unstable [16] in integrable systems, the presence of chaotic separatrix layers makes them easily observable in nonintegrable maps and flows. Finally, semi-analytic conditions for the reconnection and bifurcation of the period-three islands are obtained from the properties of the invariant curves of T^3.

2. Classification of twist functions

Regarding the twist function $f(x)$ as an unfolding of x, let

$$f(x) = P_m(x) = x - ax^2 + bx^3 + \cdots = \sum_1^m a_k x^k, \tag{7}$$

where $P_m(x)$ is a polynomial with alternating coefficients, linear term x and constant term zero. It is convenient to parametrize the coefficients of $P_m(x)$ in terms of its extrema at $\{x_i^*\}_1^{m-1}$:

$$f'(x) = \Pi_1^{m-1}(1 - x/x_i^*). \tag{8}$$

Thus

$$f(x) = \sum_{k=1}^{m} \frac{(-1)^{k+1}}{k} S_{k-1} x^k, \tag{9}$$

where $S_0 = 1$ and

$$S_k = \sum{}' \frac{1}{x_{i_1}^* x_{i_2}^* \cdots x_{i_k}^*}. \tag{10}$$

In this way one can easily construct polynomials $P_m(x)$ such that

$$0 < \min\{f(x_i^*)\} < 2\pi n < \max\{f(x_i^*)\}. \tag{11}$$

A word of caution is in order regarding cases where (7) represents a Taylor series approximation to some physical twist function. Such expansions are valid only near the origin and may introduce spurious critical points if utilized for finite values of x, even within the radius of convergence. For example, in Ref. [20] a "relativistic standard map" is derived, with monotonic

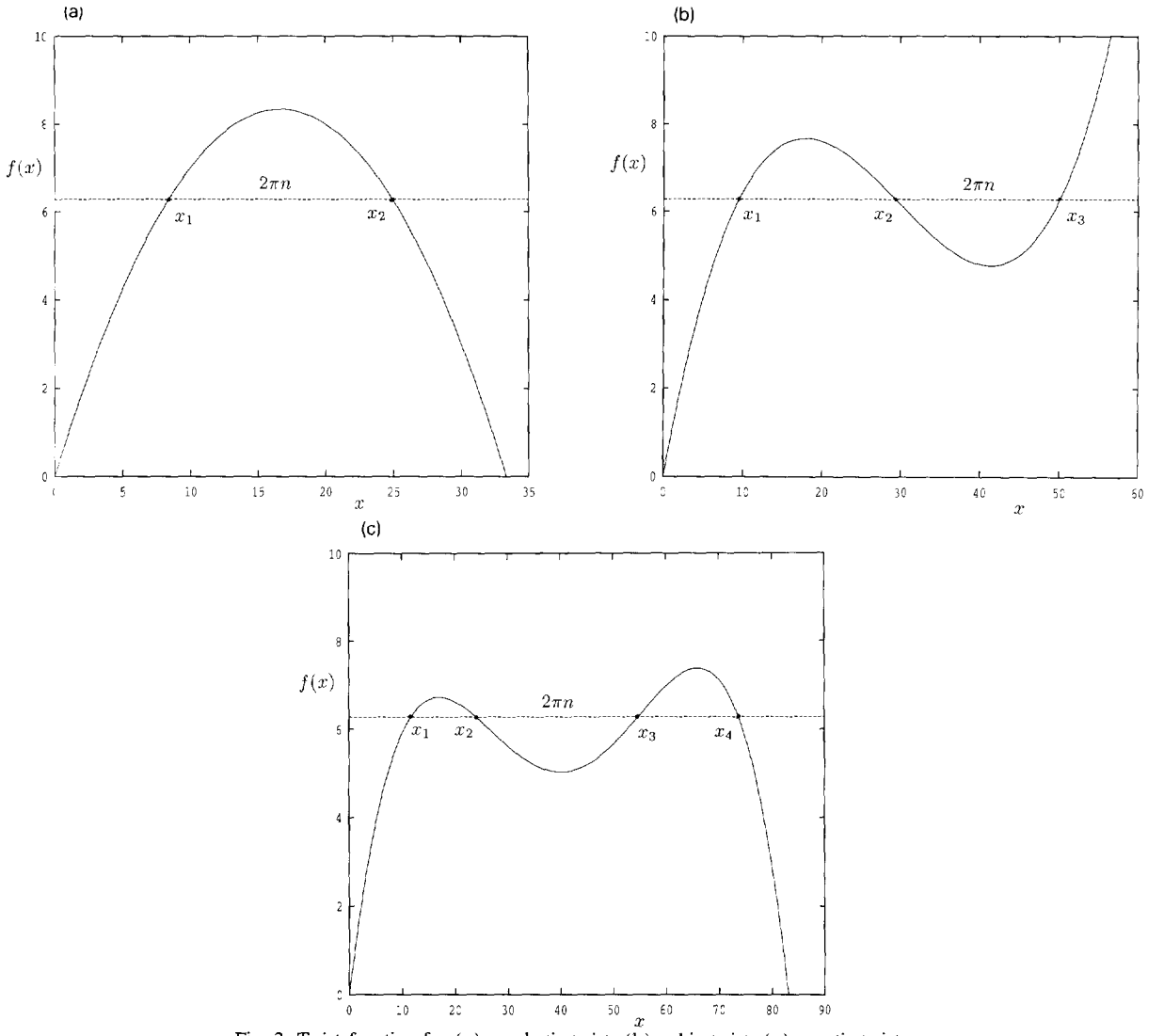

Fig. 2. Twist function for (a) quadratic twist, (b) cubic twist, (c) quartic twist.

twist function (in our notation) $f(x) = x/\sqrt{1+\beta x^2}$, which has the Taylor expansion $f(x) \approx x - \frac{1}{2}\beta x^3$. A mapping constructed from this approximate twist function would contain reconnecting structures not present in the original physical model.

Quadratic twist

For the quadratic model of Ref. [10],

$$f'(x) = 1 - x/x^*$$

so that we have the one-parameter family

$$f(x) = x - \alpha x^2 \tag{12}$$

with $\alpha = 1/2x^* > 0$, as sketched in Fig. 2a. The resonances thus occur in pairs $x_{1,2} = (1 \pm \sqrt{1 - 8\pi n\alpha})/2\alpha$, which annihilate in a tangent bifurcation (*codim 1*) when $\alpha = 1/8\pi n$. As in Ref. [10] we shall refer to the resulting map as the logistic twist map (LTM). Fig. 3 shows sections for $K = 1.5$ and two values of α, illustrating the characteristic island staggering and reconnection of KAM curves as the control parameter α passes through the critical value given by (4). The period-one fixed points are located

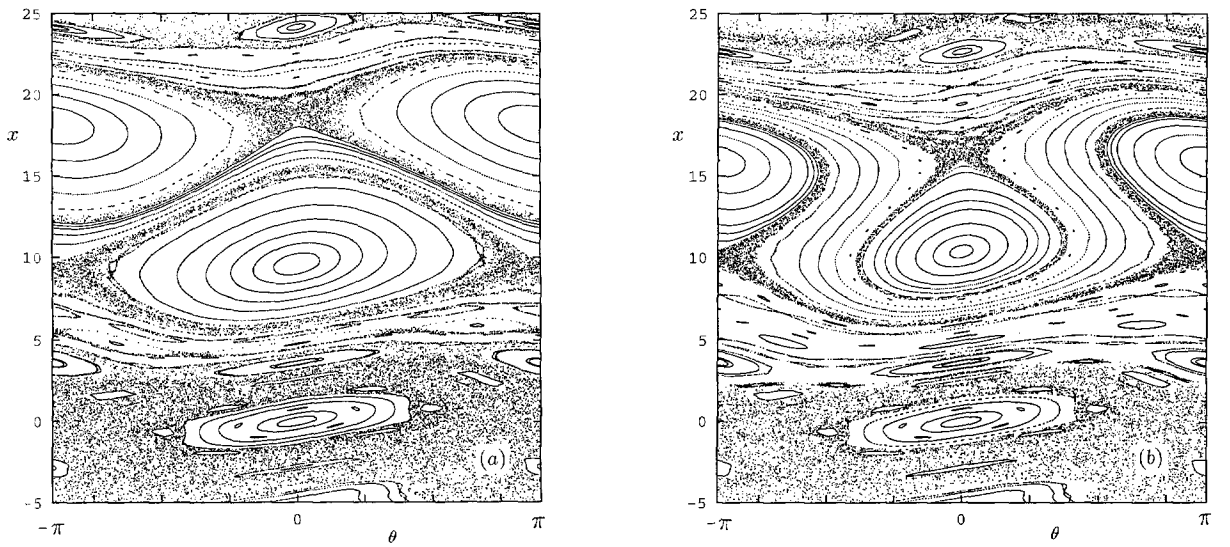

Fig. 3. Logistic twist map for $K = 1$ and (a) $\alpha = 0.036$, (b) $\alpha = 0.038$.

at the intersections of the invariant curves Γ_1 and Γ_2 of the involutions I_1 and I_2. For I_1 the curves are the vertical lines $\theta = 0, \pi$ while for I_2 we find

$$\theta = \tfrac{1}{2} f(x) - \pi m, \quad m \in Z. \tag{12a}$$

Fig. 4 shows the invariant curves for $\alpha = 0.036$ and $m = 0, 1$ (all others being equivalent mod 2π) which locate the period-one fixed points in Fig. 3a. These curves will prove useful in tracking period-two fixed points in Section 5.

Note that by the Morse Lemma [16] $f(x)$ is structurally stable to small perturbations. It follows that the fixed points of the mapping (1) are also robust and that the reconnections and bifurcations are similarly unaffected by small perturbations.

The reconnection threshold is given by evaluating the integral (4):

$$K_r(\alpha) = \frac{(1 - 8\pi n\alpha)^{3/2}}{12\alpha^2} \tag{12b}$$

and is plotted in Fig. 5 for $n = 1$. In Ref. [10] extensive comparisons were made between the predictions of (12b) and numerical calculations. The results show that (12b) is very accurate for smaller K-values but that the growth of chaotic regions and secondary islands come into play at large values of K. The lower (elliptic) fixed point period-doubles when

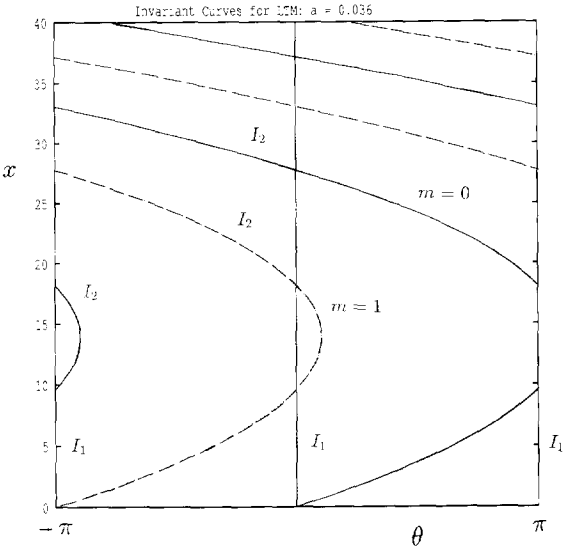

Fig. 4. Invariant curves for logistic twist map for $\alpha = 0.036$.

$Kf' = K\sqrt{1 - 8\pi n\alpha} = 4$, (a *codim 1* bifurcation), plotted in Fig. 5 as the dashed curve labelled K_{bif}. The presence of finite separatrix layers obscures the reconnection process, so that it is more accurate to speak of reconnection of a chaotic band. Here the existence of an adiabatic barrier to chaotic diffusion is intimately linked to the reconnection process. As described in Ref. [10], the meandering stream of KAM surfaces between the loops in Fig. 3b may be destroyed by in-

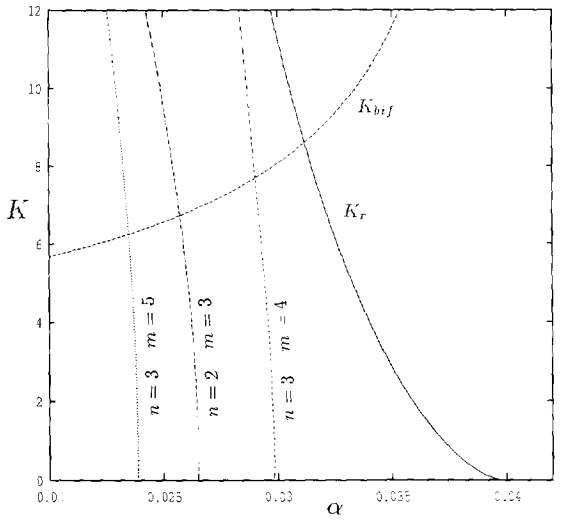

Fig. 5. Reconnection diagram for logistic twist map, including thresholds for period-two and -three islands.

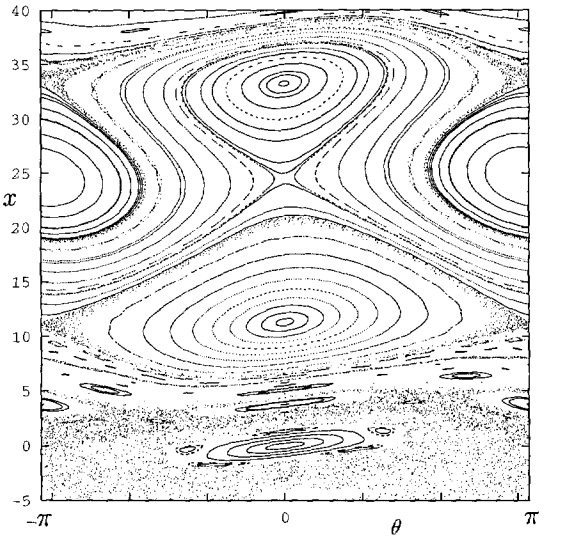

Fig. 6. Cubic twist map for $K = 1.75$, $a = 0.047$ and $b = 0.00068$.

creasing K. Note that the period-one homoclinic points are connected homoclinically after as well as before reconnection. Heteroclinic connections between neighboring pairs of resonances are possible when the intervening KAM curves have been destroyed.

In contrast, the cubic twist function described in Section 3 is a two-parameter family, which allows us to select conditions such that the effects of chaotic orbits are entirely negligible. In Ref. [10] we showed that the period-two and -three secondary islands strongly affect reconnection and destruction of adiabatic barriers to chaotic diffusion. The properties of these resonances will be elucidated and compared with their cubic analogues in Section 5.

3. Cubic twist

For a cubic twist function there are in general two extrema,

$$f'(x) = (1 - x/x_1^*)\ (1 - x/x_2^*),$$

which yields the two-parameter family

$$f(x) = x - ax^2 + bx^3, \tag{13}$$

with

$$a = \frac{x_1^* + x_2^*}{2x_1^* x_2^*}, \quad b = \frac{1}{3x_1^* x_2^*}, \tag{14}$$

both positive, as depicted in Fig. 2b. Inverting (14), we find

$$x_{1,2}^* = \frac{a \pm \sqrt{a^2 - 3b}}{3b}. \tag{15}$$

When $a^2 = 3b$ the maximum and minimum merge into a horizontal inflection point at $\bar{x} = a/3b = 1/a$, where $f(\bar{x}) = 1/3a$. In order that all three resonances exist, a and b must be chosen such that $a^2 > 3b$ and $f(x_2^*) < 2\pi n < f(x_1^*)$. A first approximation is conveniently found by letting the resonance line pass through the horizontal inflection point; $2\pi n = 1/3a$, and unfolding by decreasing b slightly from $\bar{b} = a^2/3$. Fig. 6 shows the (*codim* 2) unfolded cubic twist map (CTM) for $K = 1.75$, $a = 0.047$ and $b = 0.00068$. Varying b with a fixed then allows us to control the position of the resonance line and thereby cover the complete sequence of reconnections and bifurcations. Again, by the Morse Lemma [16] the general appearance of the mapping is stable to small perturbations that may arise in real physical systems.

In order to justify this program, let us consider the cubic resonance equation

$$bx_0^3 - ax_0^2 + x_0 - 2\pi n = 0, \quad n \in Z^+, \tag{16}$$

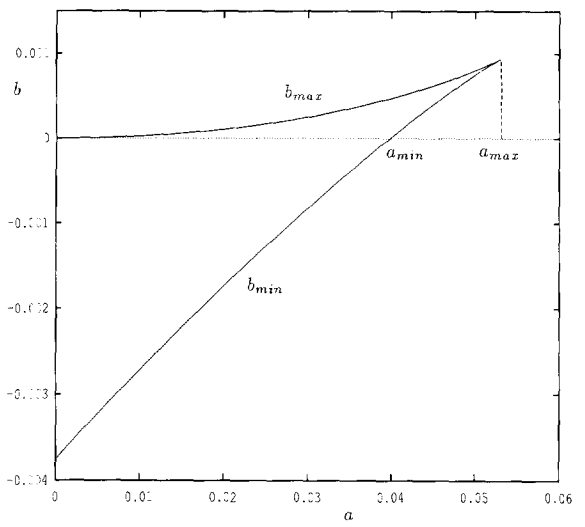

Fig. 7. Coefficients of cubic resonance equation leading to positive real resonances.

which has three positive real roots for all positive a and b. We must show that the position of the resonance line can be moved smoothly from peak to valley of $f(x)$ by varying b between two *positive* real limits, $b_{min} < b < b_{max}$. At each extremum (16) has a double root, where its discriminant vanishes. This gives

$$(a^2 - 3b)^3 = [\tfrac{9}{2}b(6\pi nb - a) + a^3]^2, \tag{17}$$

which reduces to a quadratic for b:

$$(27n^2\pi^2)b^2 - (9n\pi a - 1)b + \tfrac{1}{4}a^2(8n\pi a - 1) = 0, \tag{18}$$

whose roots (b_{min}, b_{max}) are positive real iff $a > 1/8n\pi$. The discriminant of (18) is in turn a cubic in a, which reduces to $\Delta' = (6\pi na - 1)^3$. The vanishing of Δ' at $a = 1/6\pi n$ then yields an upper bound for real values of b_{max} and b_{min}. This rather Byzantine stratification of nested cubics and quadratics is summarized in Fig. 7, which shows the useful range of b_{max} and b_{min} vs. a. When $1/8\pi n < a < 1/6\pi n$, both limits exist and are positive. Fixing a in this range and varying b then leads to a family of reconnection diagrams in the b–K plane all qualitatively similar to Fig. 4 of Ref. [10].

As in the quadratic case, accurate reconnection thresholds may be calculated from the averaged Hamiltonian (3). The result is

$$K_{12} = \tfrac{1}{2}\int_{x_1}^{x_2}[f(\xi) - 2\pi n]\,d\xi,$$

$$K_{23} = -\tfrac{1}{2}\int_{x_2}^{x_3}[f(\xi) - 2\pi n]\,d\xi,$$

$$0 = \tfrac{1}{2}\int_{x_1}^{x_3}[f(\xi) - 2\pi n]\,d\xi = K_{12} - K_{23}. \tag{19}$$

Thus, in addition to the expected braiding of contiguous islands, there is the possibility of reconnection of the upper and lower island chains when $K_{12} = K_{23}$. The complete picture is summarized in the reconnection diagram of Fig. 8, which gives the reconnection thresholds K_{12} and K_{23} in the $b-K$ plane for $a = 0.05$ and $n = 1$. The K_{12} curve begins at $b = b_{min}$, where the lower two islands annihilate in a tangent bifurcation, increasing monotonically and terminating at $b = b_{max}$, where the upper two islands annihilate. The behavior of the K_{23} threshold is similarly bounded by b_{min} and b_{max}, crossing the K_{12} curve at (b^*, K^*), in the vicinity of which it is possible for the upper and lower islands to interact. Also plotted in Fig. 8 as points are numerically derived values of K_{12} and K_{23}, which for this value of a agree with the theoretical formulas (16) to better than three significant figures. Choosing a smaller value of a leads to higher values of K, with all the complications of chaotic layers and secondary resonances. The emphasis here however, is on the discovery of new kinds of braiding.

In contrast to the quadratic case, there are several different paths in the reduced parameter space (b, K) to consider. The reconnection scenario of Fig. 9 corresponds to a path along a line of constant $K < K^*$ in Fig. 8. Starting from a point in the lower triangular region ("home base"), and travelling to the left along this path produces reconnection of the lower and middle islands, followed by mutual annihilation (not shown), while moving to the right leads to reconnection of the upper and middle islands and their ultimate demise. Both metamorphoses are locally very similar to the scenario for the quadratic twist map. The reconnection in Fig. 9a,b is shown for the full map in

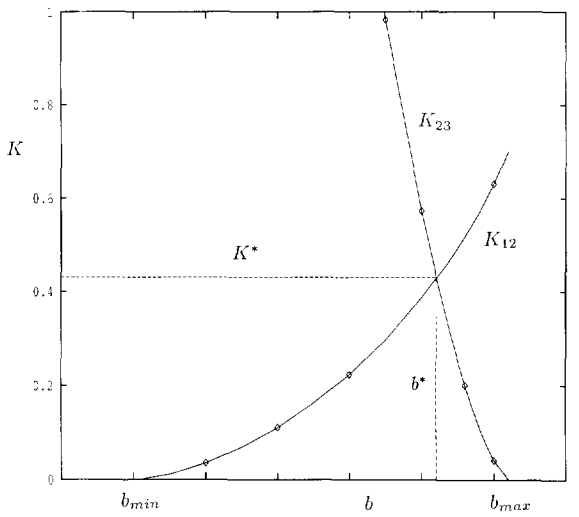

Fig. 8. Reconnection diagram for cubic twist map.

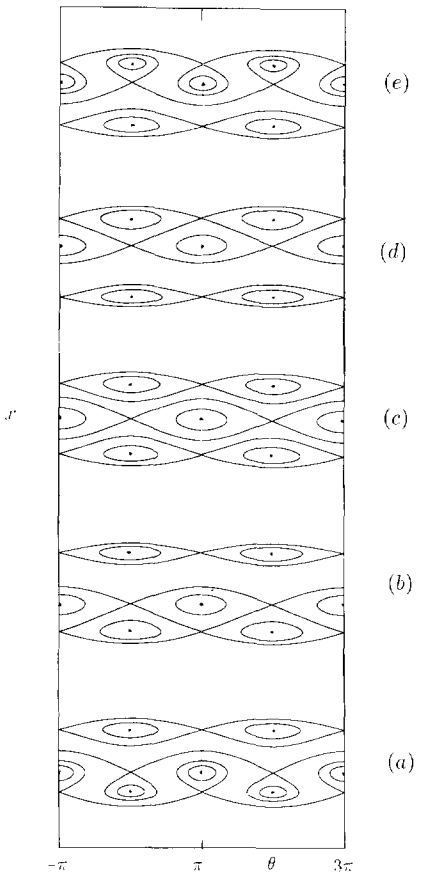

Fig. 9. Reconnection scenario for cubic twist map along a path of constant $K < K^*$.

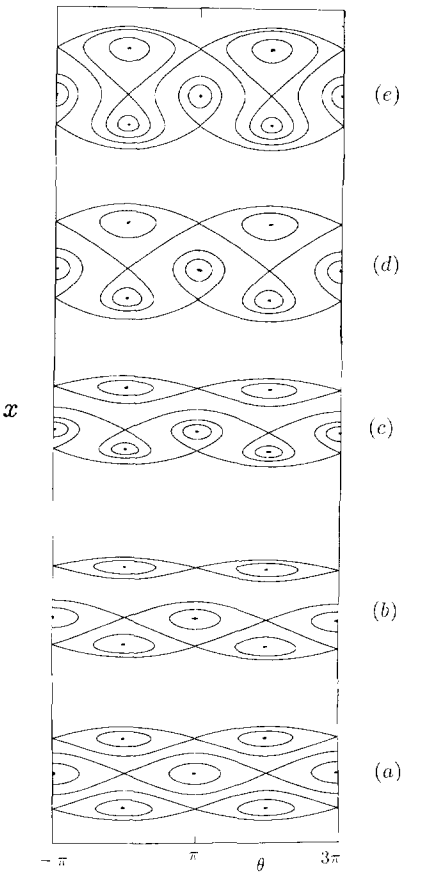

Fig. 10. Reconnection scenario for cubic twist map, along a path of constant $b < b^*$.

Fig. 6. A more interesting scenario is found along a vertical path of constant $b < b^*$, as depicted in Fig. 10. Here we observe the usual reconnection of the two lower island chains upon crossing the K_{12} threshold, followed by a second braiding of the upper two island separatrices upon crossing the K_{23} curve. Fig. 11 illustrates the strikingly beautiful hourglass structure that appears in the full mapping. A similar scenario takes place along a vertical path of constant $b > b^*$. A third type of braiding occurs for a vertical path exactly along the $b = b^*$ line, as depicted in Fig. 12. At the point (b^*, K^*) a symmetric braiding of all three island chains occurs. For $K > K^*$ the upper and lower X-points at $\theta = \pi$ are connected. Fig. 13 shows this transition for the full map, with $a = 0.05$, for which $b^* = 0.000792$, and $K^* = 0.42828$. In the integrable approximation these symmetric maps are structurally

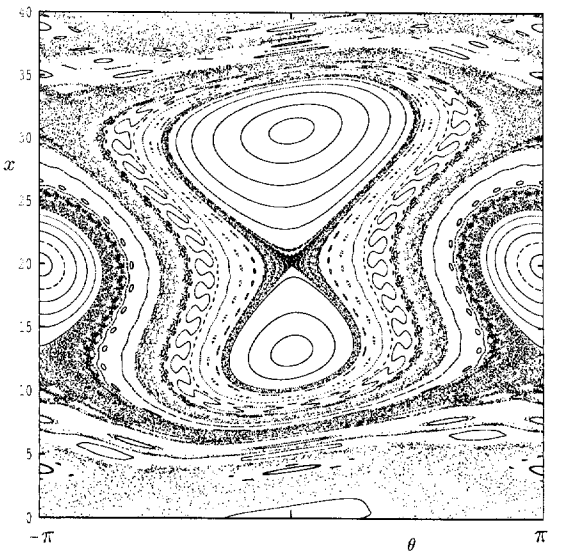

Fig. 11. Full mapping corresponding to the scenario of Fig. 9e, with $K = 2$, $a = 0.05$, and $b = 0.000785$.

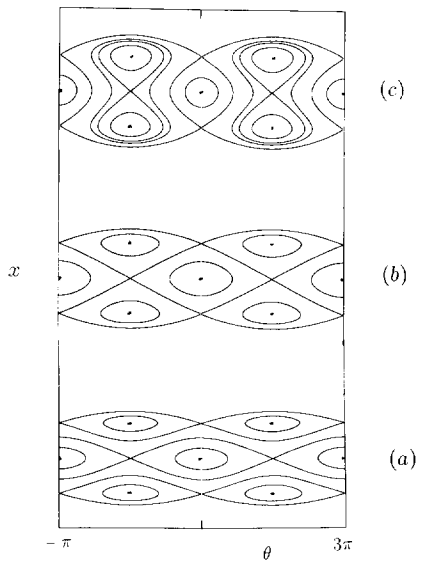

Fig. 12. Symmetric braiding for a path of constant $b = b^*$.

unstable, since a small variation in b can destroy the topology. However, the presence of a chaotic separatrix layer fuzzes out the transitions and maintains the heteroclinic connections over a finite range of b near b^*. A final scenario occurs for a horizontal path of constant $K = K^*$, where the symmetric braiding usurps the "home base" configuration seen in Fig. 9. Reconnection and bifurcation of secondary islands will be described in Section 5.

4. Quartic twist

The three-parameter twist function is

$$f(x) = x - ax^2 + bx^3 - cx^4, \tag{20}$$

with

$$2a = \frac{1}{x_1^*} + \frac{1}{x_2^*} + \frac{1}{x_3^*}, \quad 3b = \frac{1}{x_1^* x_2^*} + \frac{1}{x_1^* x_3^*} + \frac{1}{x_2^* x_3^*},$$
$$4c = \frac{1}{x_1^* x_2^* x_3^*} \tag{21}$$

again assumed all positive. A typical case is illustrated in Fig. 2c. There are several different configurations, depending on whether the resonance line crosses $f(x)$ two or four times. Without loss of generality let us assume that $x_1^* < x_2^* < x_3^*$, with $f(x_2^*) < 2\pi n < min(f(x_1^*), f(x_3^*))$. Note that, in contrast to the quadratic and cubic cases, a general quartic has no symmetry point about which $f(x)$ has definite parity. This lack of symmetry will be seen to influence the possible modes of reconnection. In order to reduce the parameter space to managable proportions, we again take the degenerate case $f' = f'' = f''' = 0$ as a point of departure. This gives the single critical point $\bar{x} = x_1^* = x_2^* = x_3^* = 3/2a$, with $b = 4a^2/9$ and $c = 2a^3/27$. Setting $f(\bar{x}) = 3/8a = 2\pi n$ then yields a first guess for a. A typical unfolding, possessing four critical points, is illustrated in Fig. 2c. As in the cubic case, all situations of interest can be achieved by fixing a and varying b and c. However, we have not yet found a way to capture the full range of possibilities by varying only one of the parameters b or c. We call the resulting map the quartic twist map (QTM).

5. Higher-order resonances

As shown in Ref. [10] higher order island chains can also reconnect and have a strong effect on the breakdown of adiabatic barriers to global diffusion. Here we elaborate on our previous treatment of the reconnection of secondary islands in the LTM and compare their characteristics with those in the CTM. Fig. 14 shows reconnection of the period-two islands in the LTM, which is seen to be quite unlike the sce-

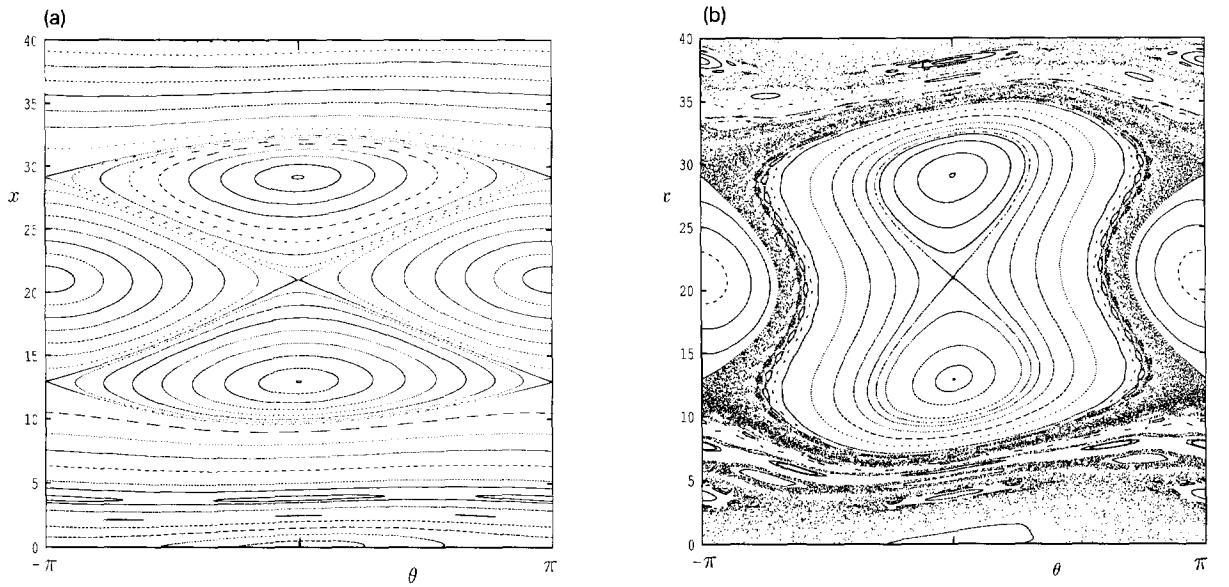

Fig. 13. Full mapping for the scenario of Fig. 12b and c.

nario for the period-one resonances. For fixed α the islands form a tight vortex-pair structure at a critical value K_2 at which the X-points momentarily merge and subsequently move apart horizontally as K is increased beyond K_2. In contrast to the transitory braiding of the period-one separatrices, however, the separatrices remain shared. As in the case of the period-one islands, the vortices annihilate in a tangent bifurcation depending only on α. The scenario for the $N = 3$ islands in the LTM more closely resembles that for the period-one islands, as depicted in Fig. 16. In general, in the LTM even-order islands form vortices and odd-order islands form loops. As we shall see, there are more possibilities in the CTM.

5.1. Period-two

In order to describe these transitions analytically, let us examine the general period-two map

$$T^2 : \begin{cases} x' &= x - K\sin\theta, \\ \theta' &= \theta + f(x'), \\ x'' &= x' - K\sin\theta', \\ \theta'' &= \theta' + f(x''), \end{cases} \tag{22}$$

whose fixed points are given by

$$f(x_0) + f(x_0') = 2\pi m, \quad m \text{ odd}, \tag{23}$$

$$\sin\theta_0 + \sin\theta_0' = 0, \tag{24}$$

or

$$\sin\tfrac{1}{2}(\theta_0 + \theta_0')\cos\tfrac{1}{2}(\theta_0 - \theta_0') = 0. \tag{25}$$

Just as for the standard map [2] there are two families of resonances, those with (i) $\theta_0 + \theta_0' = 0$ and those with (ii) $\theta_0 - \theta_0' = \pm\pi$.

Consider first the primary period-two resonances. As Fig. 14 shows, solutions are O-points at $\theta_0 = 0$, $\theta_0' = \pi$, with $x_0 = x_0'$, and X-points near $\theta = \pm\pi/2$, with $x_0' = x_0 - K\sin\theta_0$. Knowledge of the locations of these fixed points is sufficient to predict reconnection into vortex pairs and their subsequent annihilation. The locations of the O-points x_0 are easily found by setting $x_0 = x_0'$ in (23) to obtain $f(x_0) = \pi m$. Thus, for the LTM the O-points are given by $x_0 - \alpha x_0^2 = \pi m$, so that

$$2\alpha x_0 = 1 \pm \sqrt{1 - 4\pi\alpha m}. \tag{26}$$

When $\alpha = 1/4\pi m$ the $N = 2$ islands disappear in a tangent bifurcation. The positions of the O-points can also be found as the intersections of invariant curves of T^2, which can be written as a product of involutions; $T^2 = I_2(I_1 I_2 I_1) = I_2\hat{I}_1$. Alternatively, $T^2 =$

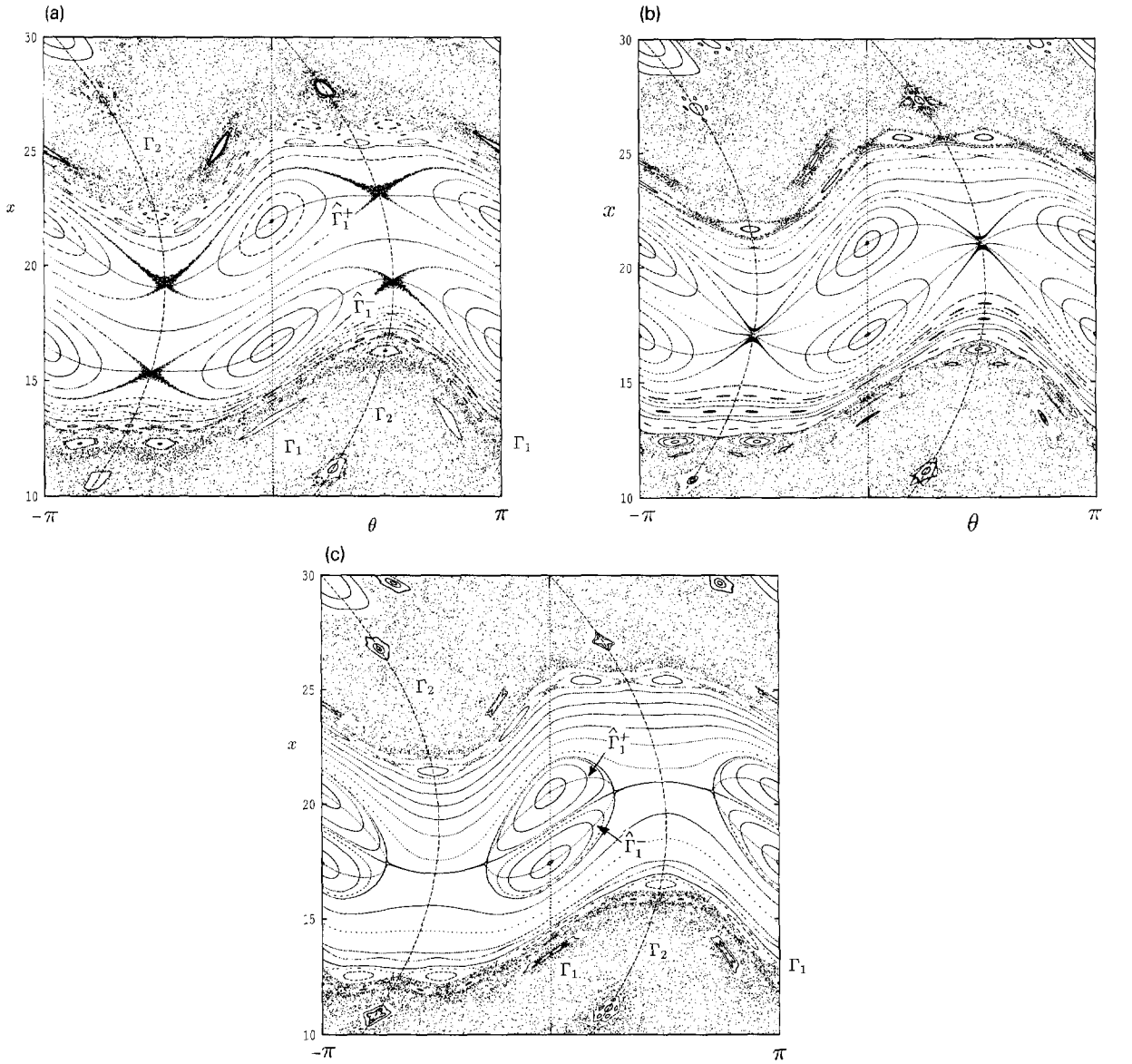

Fig. 14. Vortex pair formation in the logistic twist map, for $K = 4$ and (a), $\alpha = 0.0260$, (b) $\alpha = \alpha_c = 0.026234$, (c) $\alpha = 0.02635$. The dashed curves are invariant curves of I_1, I_2, and the resonance curves $\Gamma_r^{\pm}$.

$(I_2 I_1 I_2) I_1 = \hat{I}_2 I_1$. However, it is more convenient to utilize the "resonance curves" given by (23) and labelled by $\Gamma_r^{\pm}$ in Fig. 14. Thus, the O-points lie at the intersections of the $\Gamma_r^{\pm}$ and Γ_1, the invariant curves of I_1, which are just the vertical lines $\theta = 0, \pi$. Whether the Γ_r are themselves invariant curves of some involution remains an open question.

The X-points lie at the intersections of the resonance curves and the invariant curves of I_2. Explicitly, the Γ_r are the solutions of

$$f(x_0) + f(x_0 - K \sin\theta_0) = 2\pi m, \tag{27}$$

or

$$2\alpha x_0^2 - 2(1 + \sigma\alpha)x_0 + \sigma(1 + \sigma\alpha) + 2\pi m = 0. \tag{28}$$

where we have defined $\sigma = K \sin\theta_0$.

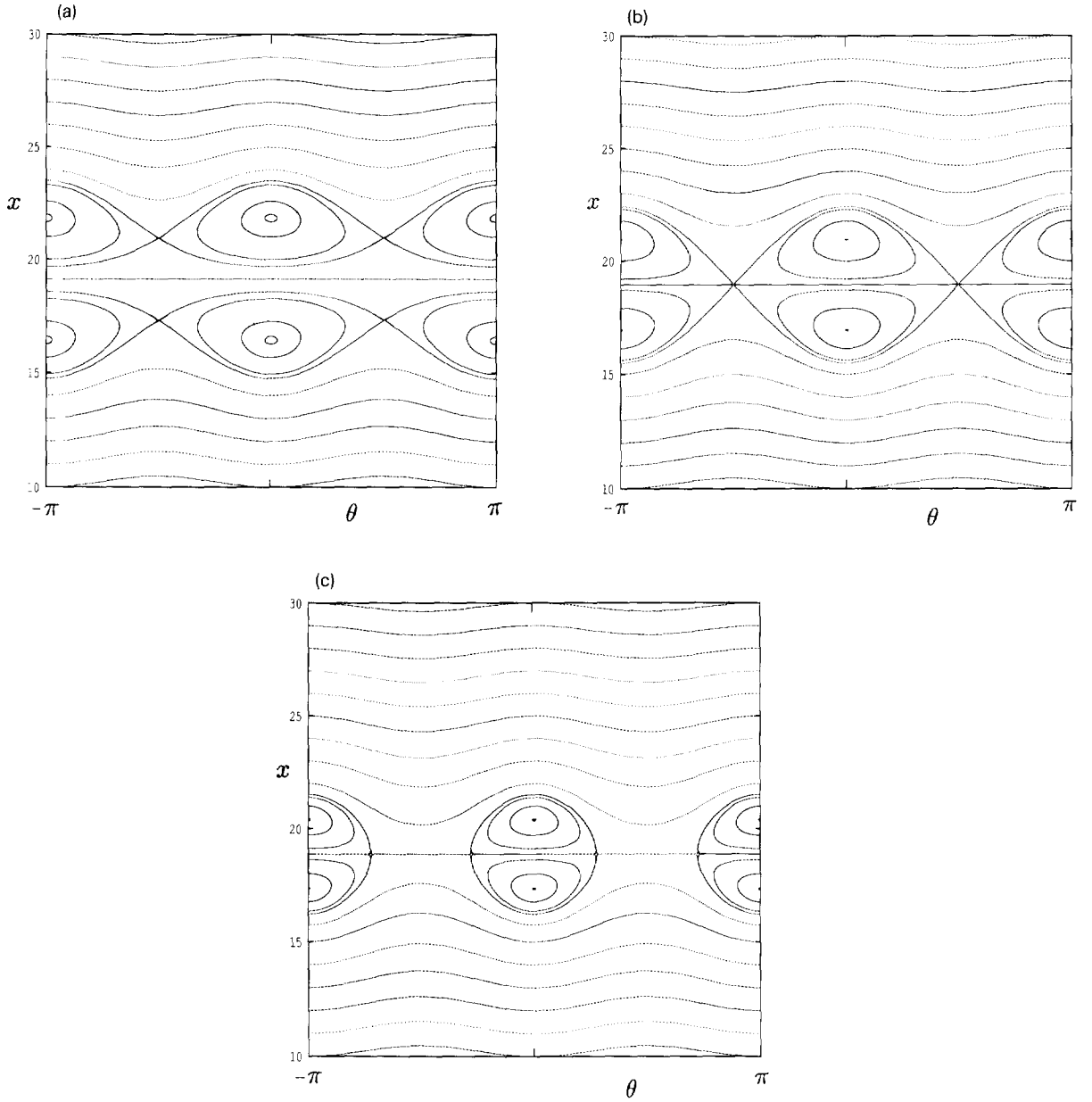

Fig. 15. Level sets for approximate integrable period-two Hamiltonian (A.17) derived using secular perturbation theory, with $K = 4$ and (a) $\alpha = 0.0262$, (b) $\alpha = 0.026378$ and (c) $\alpha = 0.0265$ (compare with Fig. 14).

The family of invariant curves associated with the involution I_2, namely

$$\theta_0 = \tfrac{1}{2} f(x_0) + \pi m, \tag{29}$$

are shown in Fig. 14 as the Γ_2 for $m = 2$ and 3. Several other resonances can also be seen to lie on Γ_2. For example, the lower island near $\theta_0 = 45^o$ is a member of an $N = 2$ pair which has bifurcated from the $N = 1$, $m = 0$ island at the origin. As noted in Ref. [10] the X-points can be made to merge, at which point a vortex pair is formed, as depicted in Fig. 14b. The X-points coincide when the discriminant of (28) vanishes:

$$\Delta = 1 - \alpha^2\sigma^2 - 4\pi\alpha m = 0 \tag{30}$$

which yields

$$\alpha K \sin\theta_0 = \pm\sqrt{1 - 4\pi\alpha m}. \tag{31}$$

Thus, there are two values of $\theta_0 \in (0, \pi)$, which merge when $\theta_0 = \pi/2$. This establishes the claim of Ref. [10] that a vortex pair is born when K exceeds

$$K_r = \sqrt{1 - 4\pi\alpha m}/\alpha, \tag{32}$$

shown in Fig. 6 as the curve labelled $N = 2$. For example, the $m = 3$ vortex pair in Fig. 14c is formed when $\alpha = 0.02623374$, $K = 4$ and disappears when $\alpha = 1/12\pi = 0.026526$. Note that the reconnection threshold (32) is derived directly from the map (19), in contrast to (4) for the period-one islands, which was derived from the approximate averaged Hamiltonian (3).

After reconnection the two branches of Γ_r join to form a single ellipsoidal curve, which no longer intersects Γ_2. The four X-points, corresponding to the stagnation points of a physical vortex pair [19], now lie at the tangential intersections of $\Gamma_r^{\pm}$, have changed symmetry type, and satisfy $\theta_0 - \theta_0' = \pi$ rather than $\theta_0 + \theta_0' = 0$. Thus, they now lie on a second pair of resonance curves $\hat{\Gamma}_r$ given by $f(x_0) = (2m - 1)\pi$, so that all X- and O-points fall on the same horizontal lines.

An approximate integrable Hamiltonian for the period-two islands can be obtained via secular canonical perturbation theory [2]. The result, as derived in Appendix A, is

$$H^{(2)} = \tfrac{1}{2}x^2 - \tfrac{1}{3}\alpha x^3 - m\pi x - \tfrac{1}{16}K^2(1 - 2\alpha x)\cos 2\theta. \tag{32a}$$

Fig. 15 shows level sets for this Hamiltonian for $K = 4$ and comparable α-values to those in the full maps of Fig. 14. The integrable flow described by $H^{(2)}$ may be useful as a model stream function for hydrodynamical vortex streets[4]. Its properties closely mimic those of the LTM for sufficiently small K; the critical point analysis of Appendix B yields reconnection and bifurcation thresholds and quantitative conditions for their applicability to the full mapping. Thus, vortex pairs form when

$$\tilde{\alpha}_{rec} = \frac{\sqrt{(4\pi m)^2 + 2K^2} - 4\pi m}{K^2} \tag{32b}$$

and disappear when

$$\tilde{\alpha}_{bif} = \frac{4\pi m - \sqrt{(4\pi m)^2 - 2K^2}}{K^2}. \tag{32c}$$

Comparing these formulas with their counterparts for the exact map shows agreement for $\alpha K^2 << 8\pi m$. For the examples of Fig. 14, $m = 3$, $\alpha \approx 0.025$ and $K = 4$, $\alpha K^2 \approx 0.4 << 24\pi$. The predicted thresholds are $\tilde{\alpha}_{rec} = 0.026378$, $\tilde{\alpha}_{bif} = 0.026677$, in good agreement with the exact values, $\alpha_{rec} = 0.026234$, $\alpha_{bif} = 0.026526$.

For the CTM the period-two islands are similar, with O-points at $\theta_0 = 0, \pi$ and X-points at $\theta_x = \pm\pi/2$ as depicted in Fig. 17. There are three island chains, with O-points given by

$$bx_0^3 - ax_0^2 + x_0 - \pi m = 0. \tag{33}$$

As in the LTM, vortex pairs disappear via a tangent bifurcation when the corresponding O-points merge, which occurs when the discriminant of (33) vanishes. Since (33) can be obtained from (16) by replacing $n \to m/2$, we may derive conditions for the existence of the $N = 2$ islands *mutatis mutandis* from the $N = 1$

[4] Although the reconnected period-two islands closely resemble vortex pairs familiar from hydrodynamics, there is an essential difference. Hydrodynamic vortices are described by *poles* of a stream function, whereas the analogous points in the level sets of $\tilde{H}^{(2)}$ are local *maxima* and *minima*.

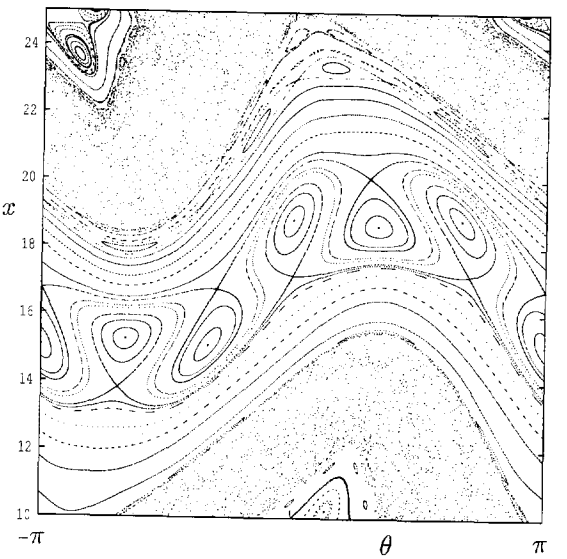

Fig. 16. Reconnection of period-three islands in the logistic twist map for $a = 0.0295$ and $K = 4.1$.

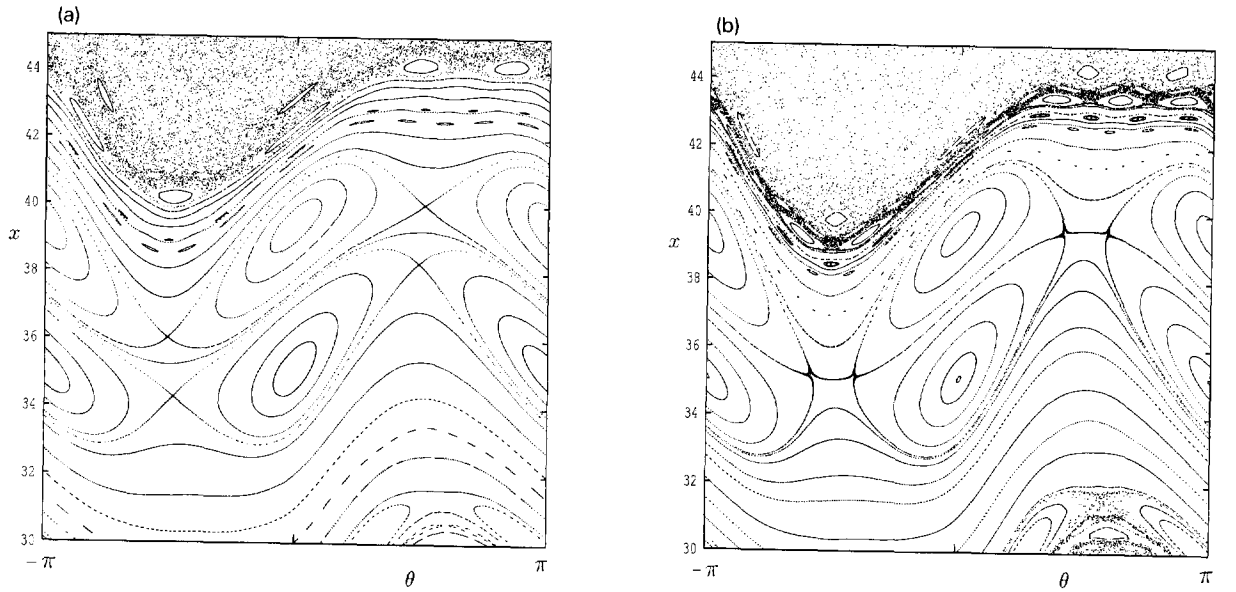

Fig. 17. Vortex pair formation in the cubic twist map for $a = 0.047, b = 0.00060$, and (a) $K = 4.0$, (b) $K = 5$.

conditions. Thus, the vortex pairs disappear when $\Delta = 0$, or

$$27m^2\pi^2b^2 - 2(9m\pi a - 2)b + a^2(4m\pi a - 1) = 0, \tag{34}$$

provided that $a^2 \geq 3b$. The solutions of (34) yield a diagram similar to Fig. 7. The vanishing of the discriminant $\Delta' = (3m\pi a - 1)^3$ gives a maximum value of a beyond which the $N = 2$ resonances cease to exist. Vortex pairs are again formed when adjacent X-points merge. The X-points are given by (27), which becomes

$$2bx_0^3 - (2a + 3\sigma b)x_0^2 + (2 + 2\sigma a + 3\sigma^2 b)x_0 - \sigma(1 + \sigma a + \sigma^2 b) - 2\pi m = 0, \tag{35}$$

whose solutions are the resonance curves Γ_r. Setting

the discriminant of (35) equal to zero yields an unwieldy quintic in b, which we have not succeeded in reducing further. Thus, an explicit threshold for vortex pair formation in the CTM may not be possible.

Now, however, there is the intriguing possibility of all three island chains simultaneously coalescing in a super-vortex. In order for this to occur, the cubic resonance curve $f(x)$ must have a shallow maximum and minimum near π. Choosing $m = 1$, we find that $f(x)$ has a horizontal inflection point at $x = 3\pi$ when $a = 1/3\pi$ and $b = a/9\pi$. For fixed a, the unfolded $f = \pi$ resonance passes through the (now oblique) inflection point when $27\pi b^2 - 9ab + 2a^3 = 0$. For $a = 0.1$ this gives $\bar{b} = 0.00316828$ and 0.0074420. The second solution is extraneous since $3\bar{b} > a^2$. In the integrable approximation, when b deviates from $\bar{b}$ a triplet does not form, i.e. *vortex triplets are structurally unstable* [16]. However, just as for the period-one resonances, the presence of chaotic separatrix layers mitigates this sensitivity.

Fig. 18 shows the spectacular vortex triplet that forms when $K \approx 4.5$. Unlike vortex pairs, the creation of a vortex triple occurs in several stages. First the upper and lower X-points undergo simultaneous tangent bifurcations, giving birth to an O-point and two neighboring X-points, as depicted in Fig. 18b. Next a complicated reconnection involving the new O-points and the central X-point takes place, similar to the period-one reconnection of Fig. 12, as illustrated in Fig. 18c. At this point the vortex triplet is also formed. It may be possible to derive an analytic threshold for this reconnection and thereby a condition for triple-vortex formation, using an averaged N=2 Hamiltonian along the lines of Appendix A. Finally, the hourglass structure disappears in an inverse tangent bifurcation, as shown in Fig. 18d. Also shown are the (dashed) invariant curves of I_1, I_2 and the Γ_r, which serve to locate (almost) all period-two fixed points, including the new O-points born near $\pm 90^o$. As in the case of the LTM vortex pairs, two of the three separate Γ_r curves in Fig. 18a join to form a single closed elliptical curve in Fig. 18b. Again, the post-reconnection X-points have changed symmetry type such that the upper O- and X-points all lie on the same horizontal line given by $f(x_0) = (2m - 1)\pi$. The vanishing of the hourglass figure corresponds to a triple root of (35) and is readily predictable analytically. For fixed a and $\bar{b}(a)$ the critical value of K is

$$K^* = \frac{2}{3\bar{b}}\sqrt{a^2 - 3\bar{b}}. \tag{36}$$

For $a = 0.1$ and $\bar{b} = 0.00316828$ this gives $K^* = 4.6829$, in good agreement with numerical calculations.

Also worthy of note is the extreme asymmetry in the chaotic layers surrounding the upper and lower heteroclinic points. While the "exterior" regions are quite chaotic, the "interior" region appears to be very regular. It would be interesting to explore the structure of the heteroclinic orbits for these points and to calculate Lyapunov exponents for the interior and exterior regions. We expect that even more complex, albeit structurally unstable, supervortices can be stacked for higher dimensional unfoldings, such as the QTM.

5.2. Period-three

The general period-three map is

$$T^3 : \begin{cases} x' &= x - K\sin\theta, \\ \theta' &= \theta + f(x'), \\ x'' &= x' - K\sin\theta', \\ \theta'' &= \theta' + f(x''), \\ x''' &= x'' - K\sin\theta'', \\ \theta''' &= \theta'' + f(x'''), \end{cases} \tag{37}$$

whose fixed points are given by

$$f(x_0) + f(x_0') + f(x_0'') = 2\pi m, \tag{38}$$

$$\sin\theta_0 + \sin\theta_0' + \sin\theta_0'' = 0, \tag{39}$$

where m is an integer not divisible by 3. Let us apply these conditions to the period-three islands in Fig. 16, which depicts the LTM for $K = 5.35$ and $\alpha = 0.0292$. Setting $\theta_0 = 0$, (39) is satisfied for $\theta_0'' = -\theta_0'$. It follows that $x_0 = x_0'$, so that (38) becomes

$$2f(x_0') + f(x_0' - \sigma) = 2\pi m, \tag{40}$$

whose solutions we call resonance curves, analogous to the $\Gamma_r^{\pm}$ for the period two islands. In addition, setting $\theta'' = -\theta'$ in the third of Eqs. (37) gives

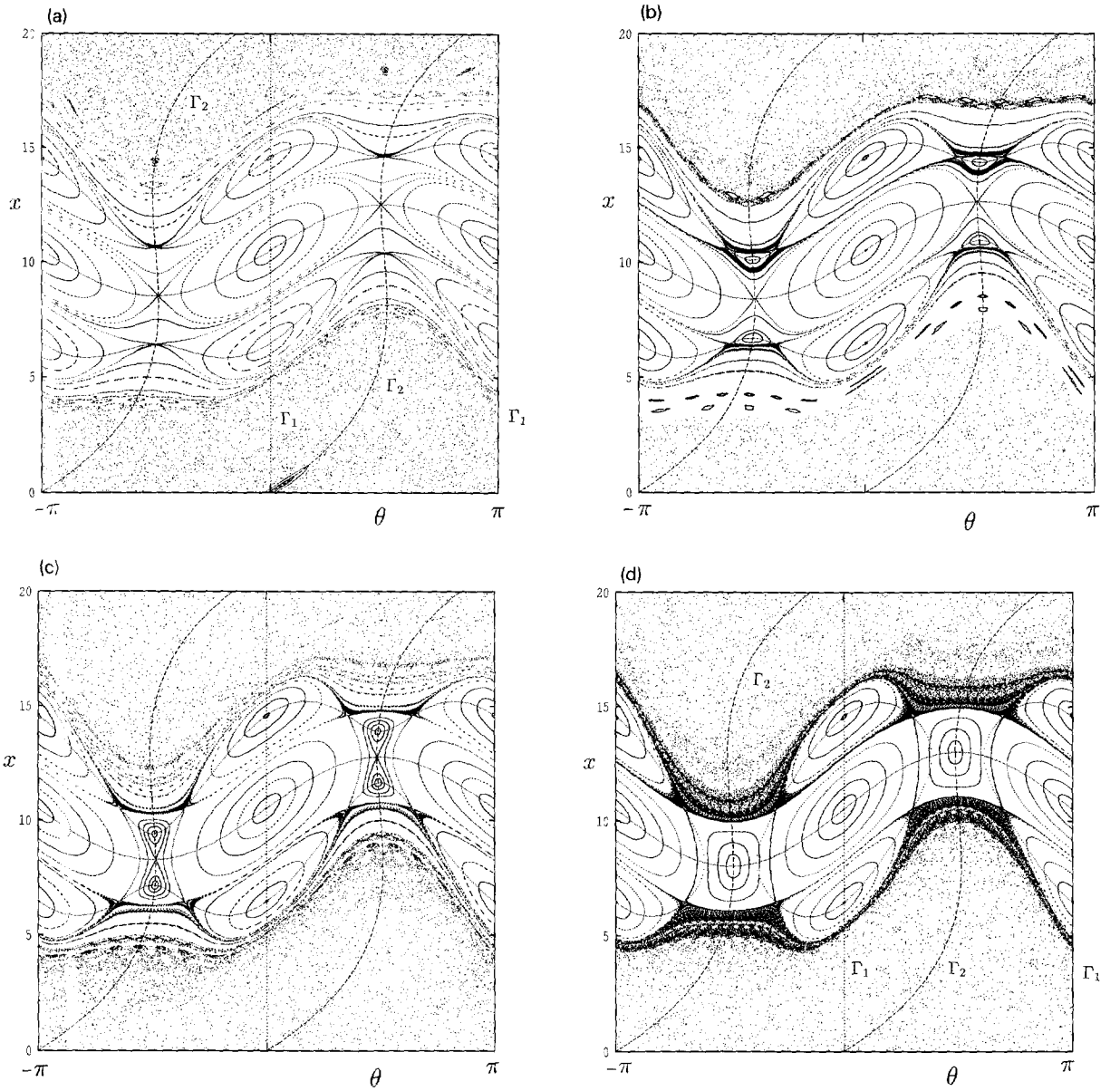

Fig. 18. Vortex triplet formation in the cubic twist map for $a = 0.1$, $\bar{b} = 0.00316828$ and (a) $K = 4$, (b) $K = 4.25$, (c) $K = 4.5$, (d) $K = 5.0$.

$$f(x_0') + 2(\theta_0' - \pi m) = 0, \tag{41}$$

which is an invariant curve of $\hat{I}_1 = I_1 T$. These curves intersect at the fixed point (x_0', θ_0'), as shown in Fig. 16. (It is readily seen that $T^3 = \hat{I}_2 \hat{I}_1$.) The upper and lower chains annihilate in a tangent bifurcation when these two curves are tangent. In this way we generate the two $\alpha - K$ curves shown in Fig. 6 for $m = 4$ and 5. For example, for $\alpha = 0.0292$ the loops disappear for $K \approx 6.6$. For the LTM, in all cases the upper and lower loops disappear together, a symmetry property apparently shared by all odd-order islands. Even-period islands always reconnect to form vortex pairs. As in the case of vortex pair formation, reconnection occurs when the two branches of Γ_r merge to form closed curves. An approximate condition for reconnection can also be derived from an approximate

period-three Hamiltonian, which can be obtained by the methods of Appendix A.

In general, families of higher order resonances may be located by observing that in the limit $K \to 0$ the resonance condition analogous to (38) becomes

$$f(x_0) = 2\pi m/n. \tag{42}$$

For each value of n the index m must be chosen relatively prime to n. In order to see reconnections the mapping parameters $a, b, c, \ldots$ must then be carefully chosen so that the resonance line (42) crosses the twist function more than once. As in the case of vortex triplets this is most easily done by starting near an inflection point of $f(x)$. In this way we have located period-three and -four reconnections for the CTM. Here the invariant and resonance curves proved invaluable in finding reconnection thresholds. Fig. 19 shows reconnection of the period three islands for fixed a and b and two values of K. Note the pronounced asymmetry in the upper and lower loops, unlike their LTM cousins seen in Fig. 16, which are of comparable size and disappear together. In contrast, for the CTM the lower loops in Fig. 19b are seen to self-destruct before the upper loops. These differences are consequences of the different symmetries of the two maps. Another striking difference is illustrated in Fig. 20, which illustrates reconnection of two staggered period-four chains in the CTM, which again occurs in stages. In contrast, the period-four (and in fact all even-period) islands in the LTM invariably form vortex pairs. Again, the different behaviors are ultimately attributable to the symmetry properties of the invariant curves of the maps. As noted elsewhere [13] the LTM is not generic; the examples considered in this paper help lead the way toward a full understanding of the range of possible modes of reconnection.

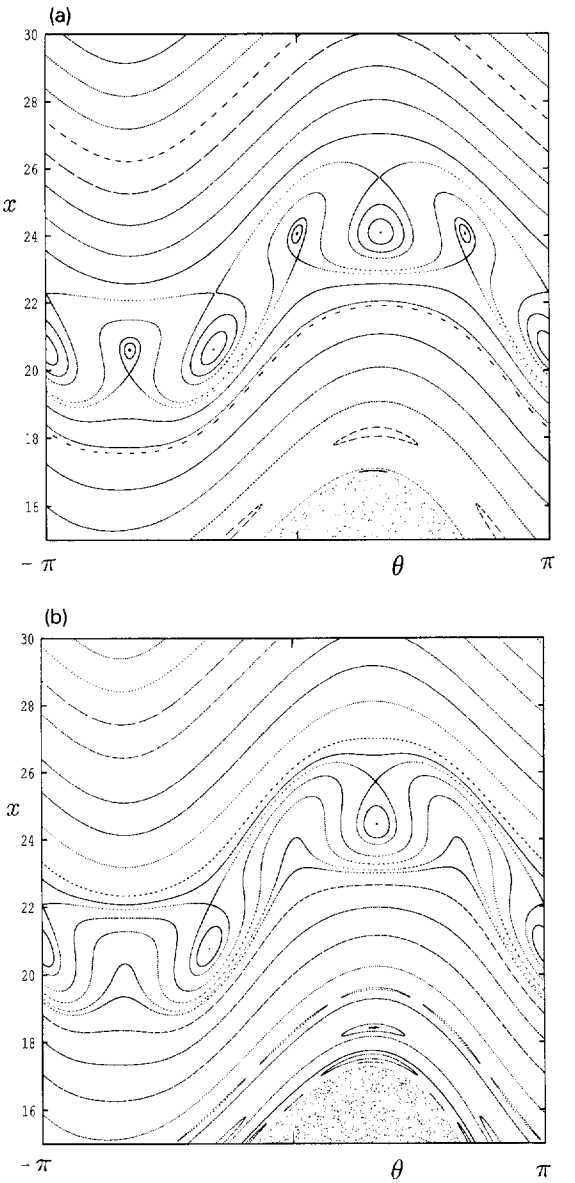

Fig. 19. Reconnection of period-three islands in the CTM for $a = 0.039$, $b = 0.000495$ and (a) $K = 4$, (b) $K = 4.25$.

6. Discussion

We have studied in some detail a new family of non-monotonic radial twist maps constructed by generalizing the linear twist function in the standard map. These mappings exhibit an extraordinary variety of novel dynamical behavior, including several new modes of reconnection. Since they were obtained as natural extensions of the linear twist function, we expect that they will model real physical systems. The relative simplicity of the mappings allows one in many cases to derive explicit analytic conditions for the observed reconnections and bifurcations as straightforward exercises in the classical theory of equations. In this way explicit conditions were derived for the reconnection and anni-

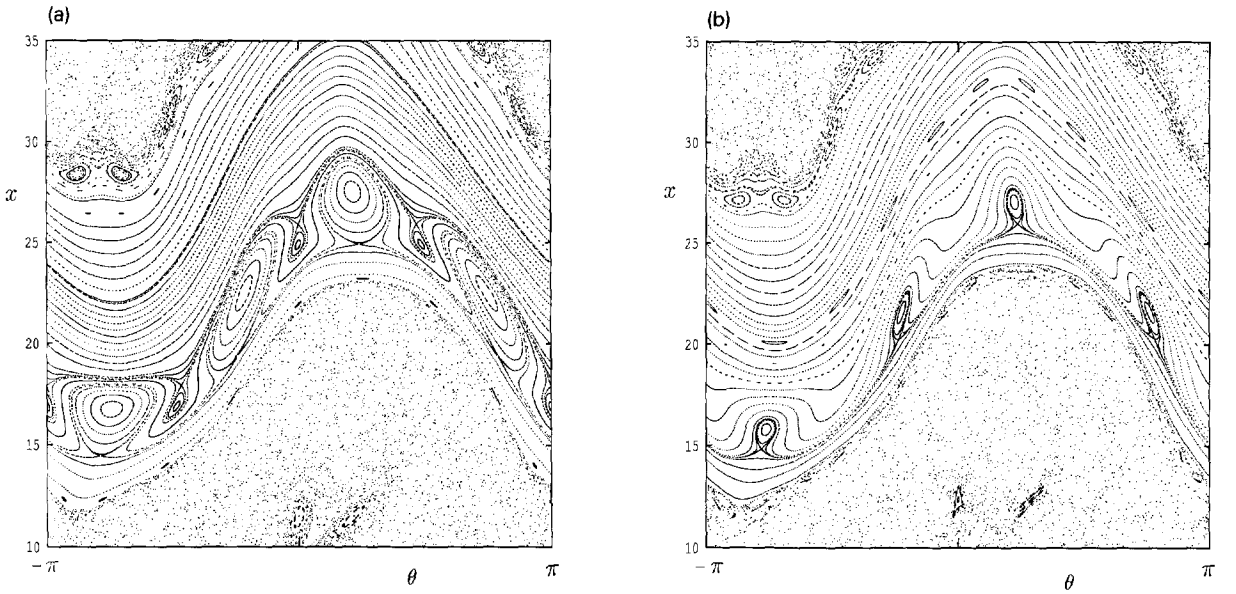

Fig. 20. Reconnection of period-four islands in the CTM for $a = 0.05, b = 0.0008$, and (a) $K = 4$, (b) $K = 5$.

hilation of both period-one and period-two resonances in the LTM, and semi-analytically for the period-three islands. For the CTM period-one islands reconnection is governed by the zeros of a quartic, which was solved numerically to generate Fig. 8. Tangent bifurcation thresholds for these resonances are given by the solutions of the quadratic (18). Vortex pairs similar to observed in two-dimensional hydrodynamic flows were found in both the LTM and CTM, and explicit reconnection and bifurcation thresholds derived for the LTM. An approximate integrable Hamiltonian for vortex pairs was derived via secular perturbation theory and shown to compare closely with the full LTM. This Hamiltonian may be useful as a model stream function for hydrodynamic vortex streets. The CTM period-three analysis was greatly facilitated by knowledge of the invariant curves. Here interesting differences were found from their LTM counterparts. While the LTM $n = 3$ islands are symmetric and annihilate together, the CTM loops are asymmetric and disappear separately. Moreover, the CTM $n = 4$ islands were found to be staggered and form asymmetric loops, unlike their LTM cousins, which are aligned and make vortex pairs. More complex higher-dimensional structures are certainly possible, but (asymmetric) loops and vortex pairs appear to be generic.

The numerical maps give one a great deal to ponder and hopefully to explain. For example, do changes of homo/heteroclinic connections invariably accompany reconnection of separatrix layers? Why are the separatrix layers so extremely asymmetric in vortex-pairs and -triplets? What does the homo/heteroclinic tangle look like in such cases? Can we generalize the mitigating effects of chaotic layers on structural instability? Are there higher-dimensional versions of reconnection? (The phenomenon was originally discovered in a four-dimensional symplectic map [4]). While all known reconnecting discrete maps are nonintegrable, physically interesting reconnecting *flows* are readily constructed. Reconnecting *integrable* flows, such as represented by the Hamiltonian (3), have been investigated for a cubic model Hamiltonian in Ref. [15]. Is a taxonomy of types of reconnection possible for two-dimensional maps or flows? The examples consider in this paper suggest an affirmative answer. The violation of the nondegeneracy conditions implies that there are regions where the Legendre transformation between the Hamiltonian and Lagrangian pictures is also violated [18]. Is a Lagrangian formulation of reconnection possible? Preliminary attempts to date have been

unsuccessful. Finally, we note that similar patterns occur in stochastic webs [21], where the nondegeneracy condition is also violated. It would be interesting to explore the parallels between nonmonotonic twist maps and the 3/2 degree of freedom models treated in Ref. [21].

Acknowledgements

We are grateful to Al Lichtenberg, Jim Meiss and Tim Poston for helpful discussions.

Appendix A. Perturbative treatment of higher order resonances

The exact Hamiltonian for the LTM can be written [2]

$$H = \tfrac{1}{2}x^2 - \tfrac{1}{3}\alpha x^3 - K\sum_{q=-\infty}^{\infty}\cos(\theta - 2\pi q n), \tag{A.1}$$

where the sum represents an infinite train of delta functions. Formally treating K as a small parameter, we seek a canonical transformation $(x,\theta) \to (\bar{x},\bar{\theta})$ such that the new averaged Hamiltonian represents the period-two resonances. Our treatment follows that of Chirikov [1] and Lichtenberg and Lieberman [2]. Taking as generating function

$$S(\bar{x},\theta,n) = \theta\bar{x} + KS_1(\bar{x},\theta,n) + K^2S_2(\bar{x},\theta,n) + \cdots, \tag{A.2}$$

where n is integer time gives

$$x = \bar{x} + K\frac{\partial S_1}{\partial\theta}, \quad \bar{\theta} = \theta + K\frac{\partial S_1}{\partial\bar{x}}. \tag{A.3}$$

Substituting (A.2) in (A.1) and collecting terms, we find

$$H = \tfrac{1}{2}\bar{x}^2 - \frac{\alpha}{3}\bar{x}^3 + K[(1-\alpha\bar{x})\bar{x}\frac{\partial S_1}{\partial\theta} + \frac{\partial S_1}{\partial n} + U] + \tfrac{1}{2}K^2(1-2\alpha\bar{x})\left(\frac{\partial S_1}{\partial\theta}\right)^2 + \mathcal{O}(K^3), \tag{A.4}$$

where U is the infinite sum in (A.1). The term proportional to K can be killed by constraining S_1 to satisfy the PDE

$$(1-\alpha\bar{x})\bar{x}\frac{\partial S_1}{\partial\theta} + \frac{\partial S_1}{\partial n} + U = 0. \tag{A.5}$$

The form of U suggests the ansatz

$$S_1(\bar{x},\theta,n) = \sum_q a_q(\bar{x})\sin(\theta - 2\pi q n) \tag{A.6}$$

so that

$$a_q = \frac{1}{(1-\alpha\bar{x})\bar{x} - 2\pi q}. \tag{A.7}$$

Hence

$$\frac{\partial S_1}{\partial\theta} = \sum_q \frac{\cos(\theta - 2\pi q n)}{(1-\alpha\bar{x})\bar{x} - 2\pi q}. \tag{A.8}$$

This yields the new Hamiltonian

$$\bar{H}(\bar{x},\bar{\theta},n) = \tfrac{1}{2}\bar{x}^2 - \frac{\alpha}{3}\bar{x}^3 + \tfrac{1}{2}K^2(1-2\alpha\bar{x})U_1(\bar{x},\bar{\theta},n), \tag{A.9}$$

where

$$U_1 = \sum_q \sum_m \frac{\cos(\theta - 2\pi qn)\cos(\theta - 2\pi mn)}{[(1-\alpha\bar{x})\bar{x} - 2\pi q]\ [(1-\alpha\bar{x})\bar{x} - 2\pi m]}. \tag{A.10}$$

To exhibit the period-two resonances, write

$$2\cos(\theta - 2\pi qn)\ \cos(\theta - 2\pi mn) = \cos[2\theta - 2\pi(q+m)n] + \cos[(q-m)2\pi n]. \tag{A.11}$$

At resonance, $\dot{\theta} = \pi(q+m) = M\pi$, M odd, so that

$$\bar{x} - \alpha\bar{x}^2 = M\pi, \tag{A.12}$$

which yields the usual pair of resonant actions. Near resonance the double sum then reduces to

$$\frac{\cos(2\theta - 2\pi n)}{2\pi^2} \sum_{m,q} \frac{1}{(M-2q)(M-2m)} = -\frac{\cos(2\theta - 2\pi n)}{8\pi^2} \sum_m \frac{1}{(m - M/2)^2} = -\tfrac{1}{8}\cos(2\theta - 2\pi n). \tag{A.13}$$

Thus we arrive at the approximate period-two Hamiltonian

$$\bar{H}^{(2)} = \tfrac{1}{2}\bar{x}^2 - \tfrac{1}{3}\alpha\bar{x}^3 - \tfrac{1}{16}K^2(1-2\alpha\bar{x})\cos(2\theta - 2\pi n). \tag{A.14}$$

where $\theta(\bar{\theta},\bar{x},n)$ is given implicitly by

$$\bar{\theta} = \theta + K(1-2\alpha\bar{x}) \sum_q \frac{\sin(\theta - 2\pi qn)}{[(1-\alpha\bar{x})\bar{x} - 2\pi q]^2}. \tag{A.15}$$

If we neglect this phase shift, $\bar{H}^{(2)}$ can be simplified by transforming to a moving frame $\hat{x}, \hat{\theta} = \theta - \pi n$ by means of the generating function

$$\hat{S}(\hat{x},\theta) = (\theta - \pi n)\hat{x} \tag{A.16}$$

Carrying out this transformation and removing the hats then gives our final result

$$\bar{H}^{(2)} = \tfrac{1}{2}x^2 - \tfrac{1}{3}\alpha x^3 - M\pi x - \tfrac{1}{16}K^2(1-2\alpha x)\cos 2\theta. \tag{A.17}$$

Appendix B. Critical point analysis of $H^{(2)}$

The critical points of the period-two LTM Hamiltonian (A.17) are given by the simultaneous solutions of

$$\frac{\partial\bar{H}^{(2)}}{\partial\theta} = \tfrac{1}{8}K^2(1-2\alpha x)\sin 2\theta = 0, \tag{B.1}$$

$$\frac{\partial\bar{H}^{(2)}}{\partial x} = x - \alpha x^2 - m\pi + \tfrac{1}{8}\alpha K^2\cos 2\theta = 0. \tag{B.2}$$

From (B.1) there are two classes of fixed points:

(*i*) $\theta_0 = 0, \pm\pi/2$, with x_0 given by

$$\alpha x_0^2 - x_0 + m\pi - \tfrac{1}{8}\sigma\alpha K^2 = 0, \tag{B.3}$$

(*ii*) $x_0 = 1/2\alpha$, with θ_0 given by

$$\tfrac{1}{8}\alpha K^2 \cos 2\theta_0 = m\pi - 1/4\alpha. \tag{B.4}$$

As in the scenario depicted in Fig. 14 let us fix K and vary α. For small α, (B.4) gives elliptic fixed points at θ_0 ($\sigma = 1$) and saddles at $\theta_0 = \pm\pi/2$ ($\sigma = -1$) located at

$$x_0^{\pm} = \frac{1 \pm \sqrt{1 - 4\alpha(m\pi - \sigma\alpha K^2/8)}}{2\alpha}, \tag{B.5}$$

which agrees with the exact values (26) for $\alpha K^2 << 8\pi m$. The O-points merge when the discriminant of (B.5) vanishes, i.e.

$$\tfrac{1}{2}\sigma K^2\alpha^2 - 4\pi m\alpha + 1 = 0, \tag{B.6}$$

so that

$$\alpha_{bif} = \frac{4\pi m - \sqrt{(4\pi m)^2 - 2K^2}}{K^2}. \tag{B.7}$$

Thus, the annihilation threshold has a slight K-dependence, in contrast to the exact value $\alpha_{bif} = 1/4\pi m$. Vortex pairs are formed when the X-points merge, i.e.

$$\alpha_{rec} = \frac{\sqrt{(4\pi m)^2 + 2K^2} - 4\pi m}{K^2}. \tag{B.8}$$

At this point the X-points lie at $x_0 = 1/2\alpha$. As α is increased further the X-points divide and move horizontally along this line, with θ_0 given by (B.4). When $\alpha \to \alpha_{bif}$, $\theta_0 \to 0$ and the vortices disappear.

References

[1] B.V. Chirikov, Phys. Rep. 52 (1979) 263.
[2] A.J. Lichtenberg and M.A. Lieberman, Regular and Chaotic Dynamics, 2nd Ed. (Springer, New York, 1992).
[3] K.R. Symon and A.M. Sessler, in: Proc. Int. Conf. on High-Energy Accelerators and Instrumentation (CERN, Geneva, 1956) p 44; A. Gerasimov, F.M. Israilev, J.L. Tennyson and A.B. Temnykh, Springer Lecture Notes in Physics, vol. 247 (1986) 154.
[4] J.E. Howard, A.J. Lichtenberg, M.A. Lieberman and R.H. Cohen, Physica D 20 (1986) 259.
[5] Diego del-Castillo-Negrete and P.J. Morrison, Phys. Fluids A 5 (1993) 948.
[6] G.D. Birkhoff, Acta Math. 50 (1927) 359.
[7] J. Guckenheimer and P. Holmes, Nonlinear Oscillations, Dynamical Systems, and Bifurcations of Vector Fields (Springer, New York, 1983).
[8] V.I. Arnold, Mathematical Methods of Mathematical Physics, 2nd Ed. (Springer, New York, 1990).
[9] V.I. Arnold, Dynamics III (Springer, New York, 1980).
[10] J.E. Howard and S.M. Hohs, Phys. Rev. A 29 (1984) 418.
[11] J.M. Greene, R.S. MacKay, F. Vivaldi and M.J. Feigenbaum, Physica D 3 (1981) 468.
[12] J.P. Van der Weele, T.P. Valkering, H.W. Capel and T. Post, Physica A 153 (1988) 283.
[13] J.P. Van der Weele and T.P. Valkering, Physica A 169 (1990) 42.
[14] T.P. Valkering and S.A. van Gils, ZAMP 44 (1993) 100.
[15] R. Egydio de Carvalho and A.M. Ozorio de Almeida, Phys. Lett. A 162 (1992) 457.
[16] T. Poston and I. Stewart, Catastrophe Theory and its Applications (Pitman, Boston, 1978).
[17] J.A.G. Roberts and G.R.W. Quispel, Phys. Rep. 216 (1992) 63.
[18] H.T. Kook and J.D. Meiss, Physica D 35 (1989) 65.
[19] G.K. Batchelor, An Introduction to Fluid Mechanics (Cambridge Univ. Press, Cambridge, 1967), Chap. 7.
[20] Y. Nomura, Y.H. Ichikawa and W. Horton, Phys. Rev. A 45 (1992) 1103.
[21] A.A. Chernikov, M. Ya. Natenzon, B.A. Petrovichev, R.Z. Sagdeev and G.M. Zaslavsky, Phys. Lett. A 129 (1988) 377.